# A detailed technoeconomic assessment of different floating solar PV types in hydroelectric dams

*Polychronakis Konstantinos[a], Sammoutos Christos[a], Vidalis Evangelos[c], Lykas Panagiotis[a],Kitsopoulou Angeliki[a], Tzivanidis Christos[a]*

[a] *National Technical University of Athens, Athens, Greece, CA:*
*polichronakis_konstantinos@mail.ntua.gr*

**Abstract:**

Floating photovoltaic (FPV) systems can expand renewable generation on hydropower reservoirs while mitigating evaporation losses, a coupled benefit of relevance to Mediterranean climates. This paper presents an integrated techno-economic, thermal, and hydrological assessment of FPV deployment on five Greek hydroelectric reservoirs, comparing water-contact membrane FPV, monofacial pontoon FPV, and bifacial pontoon FPV. An in-house MATLAB framework couples' plane-of-array irradiance, steady-state module thermal modeling, PV electrical performance, and FPV-induced evaporation reduction within a unified workflow. Technology-specific parameterizations represent water-contact heat transfer, convection over exposed structures, and bifacial rear-side irradiance, enabling consistent inter-technology comparison. Avoided evaporation is estimated from site climatic data and coverage-dependent reduction factors and converted to incremental hydroelectric generation using the effective hydraulic head.

For a fixed 5% reservoir coverage, water-contact FPV provides the largest evaporation reduction and the highest incremental hydropower benefit, reaching 639.5 MWh/year in Kremasta, whereas buoyancy-based FPV yields negligible evaporation mitigation and hydroelectric gains due to limited effective surface coverage. The techno-economic evaluation resolves component-based LCOE and IRR across the examined reservoirs. The water-based FPV achieves LCOE values of approximately 50 EUR/MWh and IRR up to 14%, while bifacial tracking maximizes PV energy yield. Overall, the findings support integrated hydro-FPV screening and design for Greek reservoirs.

**Keywords:**

Floating solar PV; Hybrid Energy Systems; Economic feasibility; Water-energy nexus.

# 1. Introduction

The transition to low-carbon power systems, together with increasing land-use constraints, has accelerated interest in floating photovoltaic (FPV) installations as an alternative to ground-mounted PV. By utilizing inland water bodies (lakes and reservoirs), FPV enables additional solar capacity without direct competition for land. In parallel, the water microclimate can reduce module operating temperature and associated thermal losses, while partial surface coverage can mitigate open-water evaporation; reported evaporation reductions span a wide range (up to 60-90%) depending on climate, coverage ratio, and platform design [1].

Deploying FPV on hydropower reservoirs is particularly attractive due to infrastructure and operational synergies. Hybrid hydro-FPV systems can reduce evaporative water losses, potentially increasing water availability during dry periods, while leveraging existing grid interconnection, access roads, and site permitting pathways [2], [3]. Nevertheless, FPV performance and project economics remain strongly site- and design-dependent, with sensitivity to meteorological conditions, reservoir geometry, and technology-specific balance-of-system requirements.

FPV concepts differ substantially in mounting approach and layout, including conventional float-based platforms, water-contact membrane systems, and tracker-enabled configurations. These design choices modify packing density (W/m$^2$ of occupied water surface), convective heat transfer, and shading patterns,

thereby affecting both energy yield and evaporation response. Consequently, evaporation mitigation cannot be represented reliably by a single generic reduction factor, because the relevant heat and mass transfer at the air-water interface depends on geometry, ventilation, and radiative shielding. Technology-resolved thermal and evaporation modeling is therefore required for consistent comparison across FPV concepts.

This paper presents a comparative techno-economic assessment of FPV deployment on five Greek hydropower reservoirs. Multiple FPV configurations with distinct mounting concepts and power-density assumptions are evaluated using site-specific meteorological forcing coupled to technology-dependent thermal and evaporation models. The analysis reports energy yield and the economic indicators LCOE and IRR, providing quantitative guidance for screening and prioritizing hydro-FPV integration in Greece.

# 2. Materials and Methods

### 2.1 Evaporation Modeling

Reservoir evaporation under baseline (uncovered) conditions was calculated using the experimentally validated regression model proposed by Bontempo Scavo et al [4]. The daily evaporation rate $E_{free}$(mm/day) is expressed as:

$$E_{free} = 2.421 + 0.012R_s + 0.159T_a - 0.056RH + 0.122U_{10} \quad (1)$$

where:

- $R_s$is the daily solar radiation (MJ/m²/day)
- $T_a$is the air temperature (°C)
- $RH$is the relative humidity (%)
- $U_{10}$is the wind speed at 10 m height (m/s)

For a floating photovoltaic (FPV) coverage ratio $x$ranging from 0 to 1, evaporation beneath FPV systems is modeled by modifying the solar radiation term with a technology-dependent factor $\kappa$:

$$E_{cov} = 2.421 + 0.012\kappa R_s + 0.159T_a - 0.056RH + 0.122U_{10} \quad (2)$$

The total lake evaporation under FPV deployment is then computed using an area-weight formulation:

$$E_{FPV} = (1 - x)E_{free} + xE_{cov} \quad (3)$$

Following Bontempo Scavo et al.[4], the technology factor $\kappa$ was set to:

- Float-based FPV: $\kappa = 1 - x$
- Water-contact membrane systems: $\kappa = 0.95x$
- Buoyancy-based structures: $\kappa = 0.2$

Daily evaporation rates were converted to volumetric water losses using the reservoir surface area.

### 2.2 Thermal Modeling

Cell temperature was calculated at each timestep using a steady-state energy balance model implemented in MATLAB following the methodology of Lindholm et al [5]. The model accounts for heat transfer processes including conduction through the module layers, convective heat exchange with the surrounding air and water environment, and longwave radiative exchange with both the sky and the water surface.

The thermal irradiance forcing is defined as:

For monofacial modules:

$$G_{th} = G_{POA,front} \quad (4)$$

For bifacial modules:

$$G_{th} = G_{POA,front} + G_{POA,rear} \quad (5)$$

Model inputs include:

- thermal irradiance $G_{th}$
- air-side wind speed $U_{air}$
- water-side wind speed $U_{water}$
- air temperature $T_a$
- water temperature $T_w$
- module tilt angle $\beta$
- evaporation rate $E$

Water temperature was approximated using the empirical relationship proposed by Ficklin et al [6].:

$$T_w = 5 + 0.75T_a \quad (6)$$

Evaporative cooling of the module was included through the heat flux term:

$$q''_{evap} = 28.4E[W/m^2] \quad (7)$$

where daily evaporation rates were assumed constant over each day, following Tina et al [7].

Convective heat-transfer coefficients were calculated using standard forced and natural convection correlations for flat plates, with air-side convection dependent on module tilt angle. Sky temperature was estimated using the Swinbank clear-sky radiation formulation [8].

The energy balance equations were solved iteratively to determine the module cell temperature $T_{cell}$, which was then used in the electrical model to obtain temperature-corrected power output.

**2.3 Solar Radiation Modeling**

Plane-of-array (POA) irradiance was calculated using solar geometry relationships combined with an isotropic transposition model. The formulation allows time-varying module tilt $\beta(i)$and azimuth $\gamma(i)$, enabling consistent representation of both fixed-tilt and tracking systems.

The front-side POA irradiance is given by:

$$G_{POA,front} = DNI \cdot max\ (0, cos\ \theta_i) + DHI \cdot \frac{1 + cos\ \beta}{2} + \rho GHI \cdot \frac{1 - cos\ \beta}{2} \quad (8)$$

where:

- $DNI$ is direct normal irradiance
- $DHI$ is diffuse horizontal irradiance
- $GHI$ is global horizontal irradiance
- $\rho$ is ground albedo
- $\theta_i$ is the incidence angle
- $\theta_z$ is the solar zenith angle

Global horizontal irradiance is computed as:

$$GHI = DNIcos\ \theta_z + DHI \quad (9)$$

Tracking angles were determined by maximizing POA irradiance within feasible orientation limits using a discrete scan algorithm.

For bifacial modules, rear-side irradiance was parameterized as:

$$G_{POA,rear} = VF_{rear}\rho GHI\frac{1-cos\ \beta}{2} + f_{diff,rear}DHI \quad (10)$$

The effective electrical irradiance is then calculated as:

$$G_{eff} = G_{POA,front} + \beta_{bf}G_{POA,rear} \quad (11)$$

### 2.4 Energy Modeling

The energy analysis combines electrical generation from FPV systems with additional hydroelectric production resulting from water savings due to reduced evaporation.

Daily energy values were used for reporting purposes, while sub-hourly data were used for coupling with the economic model.

#### 2.4.1 Reservoir Coverage and FPV Sizing

For a reservoir with surface area $A_{lake}$(km²) and FPV coverage ratio $x$(%), the installed FPV area and nominal capacity are calculated as:

$$A_{inst} = A_{lake} \times 10^6 \times \frac{x}{100} \quad (12)$$

$$P = \frac{A_{inst} \times PD}{10^6} \quad (13)$$

where $PD$ represents the power density (W/m²).

Reservoir characteristics used in the analysis are shown in Table 1, while the power density assumptions are presented in Table 2.

It should be noted that the maximum allowable FPV coverage permitted by Greek authorities for reservoirs is currently limited to 5% of the lake surface area.

#### 2.4.2 FPV Electrical Energy

For each FPV configuration $j$, electrical generation was calculated as a time series $e_{j,i}^{FPV}$(MWh per timestep) and aggregated into daily energy values $E_{j,d}^{FPV}$.

Annual energy yield is calculated as:

$$AEY_j^{FPV} = \sum_d E_{j,d}^{FPV} \quad (14)$$

***Table 1.*** *Greek reservoirs considered for FPV deployment: surface area and dam height.*

| Reservoir/lake | Area, km$^2$ | Dam height, m |
|---|---|---|
| Polyfytos | 74 | 112 |
| Kastraki | 28 | 96 |
| Pournari | 18.23 | 107 |
| Stratos | 7.4 | 26 |
| Kremasta | 80.6 | 165 |

***Table 2.*** *Power density values adopted for area-based sizing of the considered FPV configurations.*

| Type | Mount | $PD$, W/m$^2$ | Reference |
|---|---|---|---|
| Water-based FPV | membrane | 181.74 | [9] |
| Monofacial fixed-tilt | float | 160.52 | [10] |
| Monofacial tracking[1] | float | 129.03 | [10] |
| Bifacial fixed-tilt | float | 160.52 | [10] |
| Bifacial tracking[1] | float | 129.03 | [10] |
| Monofacial tracking[1] | buoy | 129.03 | [10] |
| Bifacial tracking[1] | buoy | 129.03 | [10] |
| Monofacial fixed-tilt | buoy | 220.00 | [11] |
| Bifacial fixed-tilt | buoy | 220.00 | [11] |

### 2.4.3 Hydroelectric Gain from Evaporation Savings

For each evaporation scenario $k$, daily avoided evaporation is defined as:

$$\Delta E_{k,d} = E_{free,d} - E_{FPV,k,d} \quad (15)$$

The corresponding water volume saved is:

$$\Delta V_{k,d} = 10^3 A_{lake} \Delta E_{k,d} \quad (16)$$

The resulting incremental hydroelectric energy production is calculated as:

$$E_{k,d}^{hyd} = \frac{\rho_w g H \eta_{hyd} \Delta V_{k,d}}{3.6 \times 10^9} \quad (17)$$

where:

- $\rho_w$ is water density
- $g$ is gravitational acceleration
- $H$ is the effective hydraulic head
- $\eta_{hyd}$ is the turbine-generator efficiency

### 2.4.4 Combined Energy

The total combined energy used in the economic analysis is:

$$e_{j,k,i}^{comb} = e_{j,i}^{FPV} + e_{k,i}^{hyd} \quad (18)$$

## 2.5 Economic Analysis

A discounted cash-flow model was used to evaluate the economic performance of the FPV systems. The analysis calculates the Levelized Cost of Electricity (LCOE) and the Internal Rate of Return (IRR). All monetary values are expressed in euros (EUR) and energy values in megawatt-hours (MWh).

### 2.5.1 Capital and Operational Costs

Total capital expenditure (CAPEX) is expressed as:

$$CAPEX = C_{PV} + C_{inv} + C_{cab} + C_{mount} + C_{moor} + C_{anch} + C_{comb} + C_{trk} + C_{trf} \quad (19)$$

where each term represents the cost of PV modules, inverters, cabling, floating structures, mooring systems, anchors, combiner boxes, tracking systems, and transformers respectively. Unit cost values used in this study are summarized in Table 3.

***Table 3.*** *CAPEX component unit costs used* ***Σφάλμα! Το αρχείο προέλευσης της αναφοράς δεν βρέθηκε.*** *(EUR/MW unless otherwise stated).*

| Component | Symbol | Unit cost | Reference |
|---|---|---|---|
| PV modules (monofacial) | $C_{PV}$ | 140,000 | [12] |
| PV modules (bifacial) | $C_{PVB}$ | 185,000 | [12] |
| Inverters (low–high) | $C_{inv}$ | 110,000-133,000 | [12] |
| Internal cabling | $C_{cab}$ | 14,000 | [12] |
| Floating structure (pontoon FPV) | $C_{mount}$ | 980,837 | [12] |
| Water-contact membrane (polymer film) | $C_{film}$ | 500,000 | [12] |
| Mooring lines | $C_{moor}$ | 2,880-12,958 EUR/m | [13] |
| Anchors | $C_{anch}$ | 33,920-64,375 EUR/unit | [13] |
| Combiner boxes (low–high) | $C_{comb}$ | 1,500-2,287 | [12] |
| Transformer | $C_{trans}$ | 43,668 | [12] |
| Horizontal 1 axis-Tracker (low-high) | $C_{trkH}$ | 154,260-799,880 | [12] |
| Vertical 1 axis-Tracker (low-high) | $C_{trkV}$ | 399,940-1,062,700 | [12] |
| Dual axis-Tracker (low-high) | $C_{trkD}$ | 685,610-2,171,110 | [12] |

Annual operational expenditure (OPEX) is escalated over time according to:

$$OPEX_t = OPEX_1(1 + g_{om})^{t-1} \quad (20)$$

where $g_{om}$is the annual escalation rate.

### 2.5.2 Levelized Cost of Electricity

The LCOE is calculated as:

$$LCOE = \frac{CAPEX + \sum_{t=1}^{n} OPE\,X_t DF_t + C_{EOL} DF_n}{\sum_{t=1}^{n} E_t\,DF_t} \quad (21)$$

where:

- $E_t$is the annually exported energy

- $DF_t = (1 + r)^{-t}$is the discount factor
- $r$is the discount rate
- $n$is the project lifetime
- $C_{EOL}$represents end-of-life costs.

### 2.5.3 Internal Rate of Return

Cash flows are defined as:

$$CF_0 = -CAPEX \quad (22)$$

$$CF_t = R_t - OPEX_t \quad (23)$$

The internal rate of return $r^*$is obtained from:

$$\sum_{t=0}^{n} \frac{CF_t}{(1+r^*)^t} = 0 \quad (24)$$

# 3. Results

### 3.1 Water Savings and Hydroelectric Energy Gain

Figure 1 illustrates simulated daily evaporation rates for the baseline free-water surface and for the examined FPV mounting concepts over a representative period. The results indicate that the water-contact (membrane) mounting concept produces the strongest reduction in daily evaporation, offering a clear advantage in evaporation mitigation compared with the other FPV concepts.

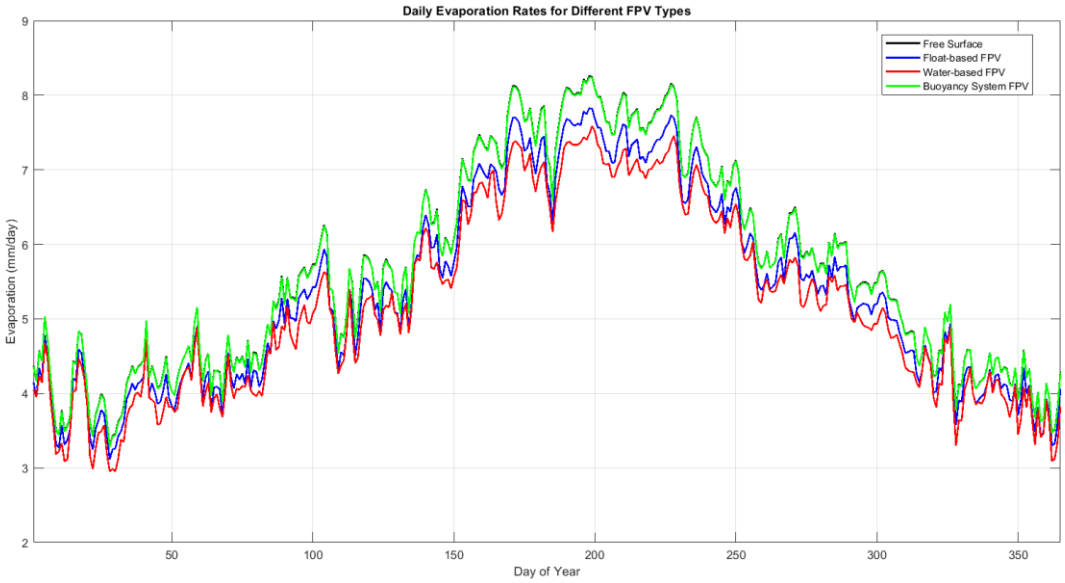


***Figure. 1: Simulated daily evaporation rates for the baseline (free surface) and FPV mounting concepts (representative period)***

Table 4 summarizes annual evaporation volumes for a fixed FPV coverage of 5% of the reservoir surface. Across all five reservoirs, the water-contact FPV concept results in the lowest annual evaporation, followed by conventional float-based systems. In contrast, the buoyancy-based concept leads to values that are almost identical to the baseline case, indicating minimal evaporation reduction.

***Table 4. Annual water evaporation for baseline conditions and for 5% reservoir coverage by FPV (million m³).***

| Reservoir | Free | Float-based | Water-based | Buoyancy-based |
|---|---|---|---|---|
| Pournari | 70.28 | 66.7 | 65.49 | 70.22 |
| Kastraki | 112.89 | 107.24 | 107.02 | 112.88 |
| Stratou | 16.57 | 15.71 | 15.15 | 16.54 |
| Polyfytou | 144.13 | 136.65 | 131.76 | 143.9 |
| Kremasta | 167.11 | 158.42 | 152.38 | 166.83 |

The annual water savings relative to the baseline are presented in Table 5. For the 5% coverage scenario, the water-based concept achieves the highest savings in all reservoirs, particularly in large-area systems. For example, water savings reach 12.37 million m³/year in Polyfytou and 14.73 million m³/year in Kremasta. Float-based systems yield moderate savings, while buoyancy-based systems provide negligible savings (below 0.28 million m³/year across all reservoirs).

***Table 5. Annual water savings relative to baseline for 5% reservoir coverage by FPV (million m³).***

| Reservoir | Float-based | Water-based | Buoyancy-based |
|---|---|---|---|
| Pournari | 3.58 | 4.79 | 0.06 |
| Kastraki | 5.66 | 5.88 | 0.01 |
| Stratou | 0.86 | 1.41 | 0.03 |
| Polyfytou | 7.48 | 12.37 | 0.23 |
| Kremasta | 8.69 | 14.73 | 0.28 |

Water savings were translated into incremental hydroelectric generation using the hydraulic head and turbine-generator efficiency described in the Energy Modeling section. Table 6 reports the resulting annual hydropower gains. Reservoirs combining large surface area with substantial hydraulic head show the greatest benefits. Under 5% coverage, the water-based concept achieves 364.73 MWh/year in Polyfytou and 639.53 MWh/year in Kremasta. By contrast, buoyancy-based configurations remain below 12.23 MWh/year in all cases, consistent with their minimal evaporation reduction.

***Table 6. Annual hydroelectric energy gain from avoided evaporation for 5% reservoir coverage (MWh).***

| Reservoir | Float-based | Water-based | Buoyancy-based |
|---|---|---|---|
| Pournari | 100.84 | 134.97 | 1.59 |
| Kastraki | 142.92 | 148.44 | 0.26 |
| Stratou | 5.88 | 9.67 | 0.18 |
| Polyfytou | 220.41 | 364.73 | 6.73 |
| Kremasta | 377.36 | 639.53 | 12.23 |

**3.2 Technoeconomic Comparison**

For the technoeconomic part of the study, we compared the annual energy yield, the LCOE and the IRR between the 17 different cases for each of the 5 lakes.

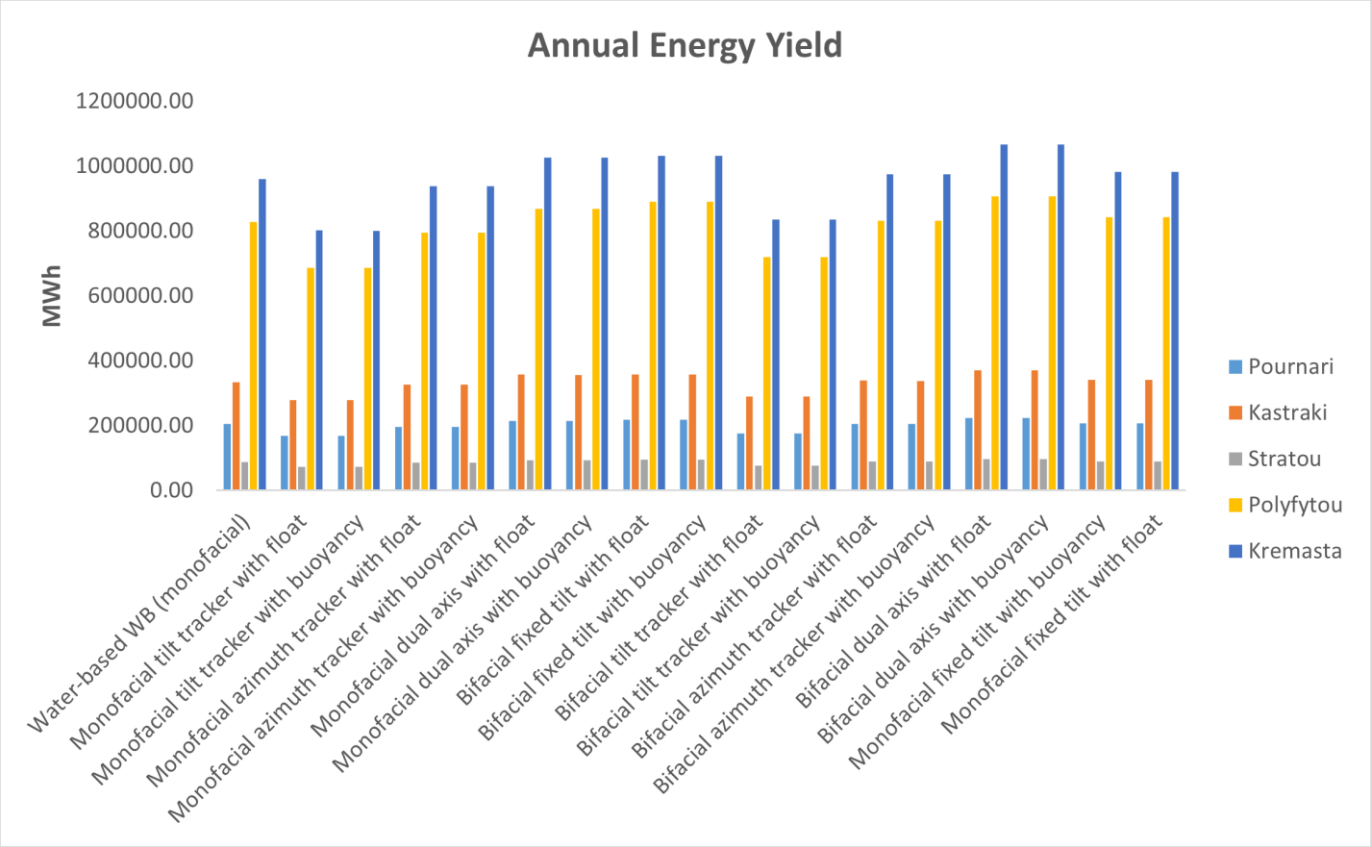


***Figure. 2a: Annual energy yield (AEY) across configurations and reservoirs.***

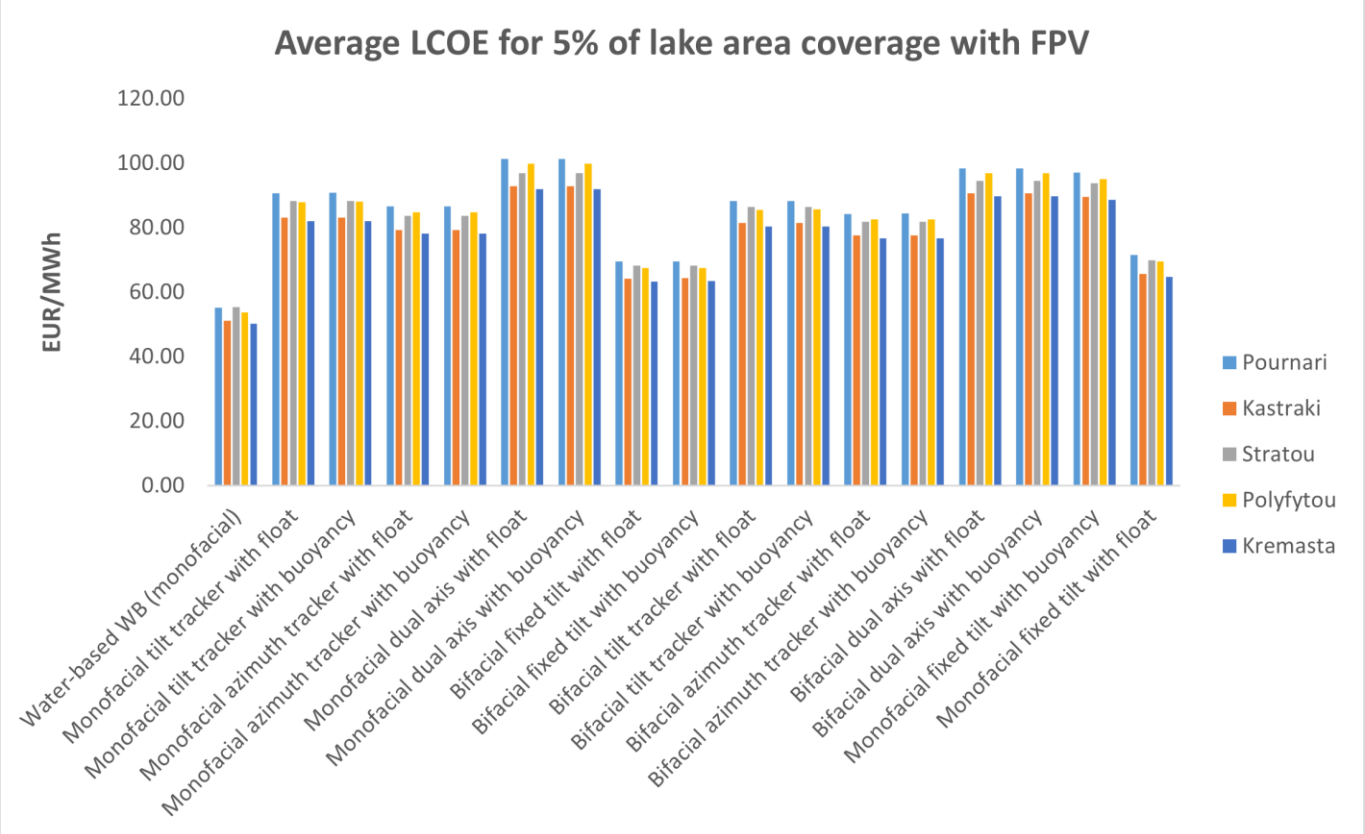

***Figure. 2b: Levelized cost of electricity (LCOE) across configurations and reservoirs.***

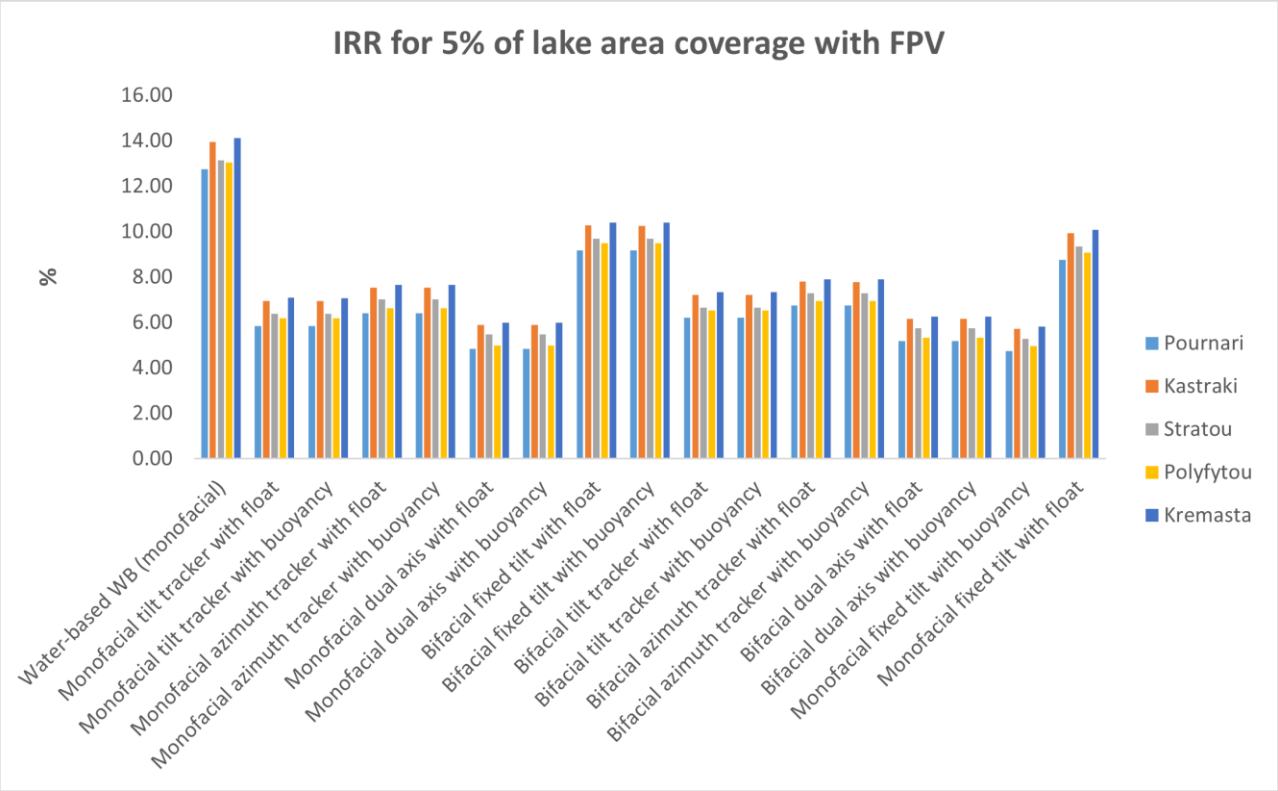


***Figure. 2c: Internal rate of return (IRR) across configurations and reservoirs.***

***Figure. 2: Electric-energy and economic indicators for the examined FPV configurations and reservoirs.***

Figure 2a reports the annual FPV electricity yield by configuration. The ranking is primarily governed by the effective irradiance (tracking and bifaciality) and by the assumed packing density (Table 2), which determines installed capacity per unit reservoir area. In this dataset, bifacial tracking configurations achieve the highest AEY across all reservoirs, while lower packing densities in some tracking layouts reduce the area-normalized yield relative to fixed-tilt cases.

Figure 2b summarizes LCOE results derived from discounted lifetime costs and discounted energy output. Water-based FPV yields the lowest LCOE in all reservoirs, reflecting (i) reduced balance-of-system cost assumptions for the mounting concept and (ii) lower operating cell temperature, which increases energy production. Float-based systems yield intermediate LCOE, whereas tracking configurations can exhibit higher LCOE when additional CAPEX (tracking hardware and structural requirements) is not compensated by the incremental electricity yield at the examined sites.

Figure 2c presents the corresponding IRR. The highest IRR values are obtained for water-based FPV and for fixed-tilt float-based systems, indicating that cost structure dominates profitability under the present assumptions. Kremasta lake exhibits the largest IRR across most configurations, consistent with its large available surface area and high hydraulic head, which jointly increase both PV scale effects and the monetizable value of avoided evaporation.

**4. Conclusion**

This study evaluated FPV deployment on five Greek hydropower reservoirs using coupled thermal, hydrological, and technoeconomic modeling, quantifying impacts on evaporation, incremental hydropower, LCOE, and IRR.

Key conclusions are summarized as follows:

1. Under 5% reservoir coverage, water-contact (membrane) FPV achieves the largest evaporation reduction and the highest incremental hydropower benefit, reaching up to 639.53 MWh/year in Kremasta.
2. Buoyancy-based FPV concepts provide negligible evaporation mitigation and correspondingly small hydropower gains due to limited effective surface shielding.
3. Water-based FPV yields the lowest LCOE (approximately 50 EUR/MWh) and among the highest IRR values (approximately 14%) across reservoirs, reflecting lower mounting-system cost assumptions and improved module cooling.
4. Bifacial tracking maximizes PV energy yield, but its economic attractiveness depends on site conditions and the relative cost premium of tracking systems.

# References


[1] L. W. Farrar, A. S. Bahaj, P. James, A. Anwar, and N. Amdar, “Floating solar PV to reduce water evaporation in water stressed regions and powering water pumping: Case study Jordan,” *Energy Convers. Manag.*, vol. 260, p. 115598, 2022, doi: 10.1016/j.enconman.2022.115598.

[2] E. Rosenlieb, M. Rivers, and A. Levine, “Floating photovoltaic technical potential: A novel geospatial approach on federally controlled reservoirs in the United States,” *Sol. Energy*, vol. 287, p. 113177, 2025, doi: 10.1016/j.solener.2024.113177.

[3] S. Z. M. Golroodbari *et al.*, “Pooling the cable: A techno-economic feasibility study of integrating offshore floating photovoltaic solar technology within an offshore wind park,” *Sol. Energy*, vol. 219, pp. 65–74, 2021, doi: 10.1016/j.solener.2020.12.062.

[4] F. Bontempo Scavo, G. M. Tina, and S. Nizetic, “An assessment study of evaporation rate models on a water basin with floating photovoltaic plants,” *Int. J. Energy Res.*, 2020, doi: 10.1002/er.5170.

[5] D. Lindholm, T. Kjeldstad, J. Selj, E. S. Marstein, and H. G. Fjær, “Heat loss coefficients computed for floating PV modules,” *Prog. Photovolt.*, vol. 230, p. 111234, 2023, doi: 10.1002/pip.3451.

[6] D. L. Ficklin, Y. Luo, I. T. Stewart, and E. P. Maurer, “Development and application of a hydroclimatological stream temperature model within the Soil and Water Assessment Tool,” *Water Resour. Res.*, vol. 48, no. 1, 2012, doi: 10.1029/2011WR011256.

[7] G. M. Tina, F. Bontempo Scavo, L. Merlo, and F. Bizzarri, “Analysis of water environment on the performances of floating photovoltaic plants,” *Renew. Energy*, vol. 175, pp. 281–295, 2021, doi: 10.1016/j.renene.2021.04.082.

[8] W. C. Swinbank, “Long-Wave Radiation from Clear Skies,” *Q. J. R. Meteorol. Soc.*, vol. 89, pp. 339–348, 1963, doi: 10.1002/qj.49708938105.

[9] Alotta, “Floating solar solutions (product information).” 2025. [Online]. Available: https://www.alotta.no/

[10] “Floating solar photovoltaics: A review of engineering, environmental, and economic aspects,” *Environ. Sustain. Indic.*, 2023, doi: 10.1016/j.esd.2023.101283.

[11] Ciel & Terre, “WATTRAK Floating Solar Solution: Maximum Density.” 2025. [Online]. Available: https://ciel-et-terre.net/wattrack-ciel-terre-solution-floating-solar-maximum-density/

[12] *J. Mar. Sci. Eng.*, vol. 13, no. 8, p. 1404, 2025, doi: 10.3390/jmse13081404.

[13] *Renew. Energy*, p. 122981, 2025, doi: 10.1016/j.renene.2025.122981.